Energy-Conserving Lattice Boltzmann Thermal Model in Two Dimensions

Benjamin Piaud,[1,2] **Stéphane Blanco,**[1] **Richard Fournier,**[1] **and Michael J. Clifton**[2]

A discrete velocity model is presented for lattice Boltzmann thermal fluid dynamics. This model is implemented and tested in two dimensions with a finite difference scheme. Comparison with analytical solutions shows an excellent agreement even for wide temperature differences. An alternative approximate approach is then presented for traditional lattice transport schemes.

KEY WORDS: Thermal lattice Boltzmann; compressibility; BGK approximation; Gauss–Hermitte quadrature.

1. INTRODUCTION

Over the last decade, it has been demonstrated that the lattice Boltzmann method (LBM) is an effective approach method for simulating a wide variety of isothermal fluid flows.(1) In the case of thermal fluid flows, LBM with a multi-speed approach under a single-relaxation-time BGK approximation,(2) suffers from numerical instabilities.(3) To avoid these instabilities, the passive scalar approach(4) or introduction of a separate thermal distribution(5) can be used. Vahala *et al.*(6) have proposed a multi-speed model with a higher-order-isotropy velocity model and multiple relaxation times to stabilize the numerical scheme and to have a variable Prandtl number. In ref. 6 a model was suggested based on Gauss–Hermite

[1]Laboratoire d'Energétique EA 810, Université Paul Sabatier, 118 route de Narbonne, 31062 Toulouse Cedex, France; e-mail: piaud@energetique.ups-tlse.fr
[2]Laboratoire de Génie Chimique UMR 5503, Université Paul Sabatier, 118 route de Narbonne, 31062 Toulouse Cedex, France.

quadrature that is a straightforward extension of the *a priori* derivation of the lattice Boltzmann equation by He and Luo.[7,8] To include thermal effects, heat conduction and viscous heat dissipation, the quadrature must be used to evaluate the moments of f to the eighth order. So the lattice Boltzmann thermal model needs five discrete velocities in one dimension and 25 discrete velocities in two dimensions.

In this work, we test different ways of implementating the proposed approach. The main difficulty arises from the fact that the quadratures are based on the equilibrium distribution function, which introduces an explicit temperature dependence. So the set of discrete velocities resulting from the quadrature is spatially inhomogeneous. To overcome this difficulty several solutions can be envisaged. As far as the macroscopic velocity is concerned, this constraint is removed by a "low-Mach-number" type of approximation. If a development equivalent to "low-Mach-number" is derived for small temperature differences, a formulation is obtained that would require, to ensure a precision equivalent to the Chapman–Enskog expansion, the exact evaluation of moments up to order 10 (cf. Appendix A). We have not chosen this solution, rather we propose adapting the quadradrature to 25 discrete velocities by choosing a reference temperature for the evaluation of the velocity modules and we take account of the temperature variations by systematically recalculating the weight factors. This system was implemented using a finite-difference scheme and has been validated for a series of academic examples that show that the scheme performs very well even for quite wide temperature differences. The second part of this work shows the difficulties involved in the implementation of this velocity discretization within a traditional lattice-transport approach. The various possibilities in this direction are explained and a first series of tests is presented.

2. DISCRETE VELOCITY MODEL FOR THERMAL APPLICATIONS

In this section, a velocity space discretization is presented for the Boltzmann equation under the BGK approximation:[2]

$$\frac{\partial f}{\partial t} + \mathbf{v} \cdot \nabla f = -\frac{1}{\tau}(f - g), \tag{1}$$

where $f \equiv f(\mathbf{r}, \mathbf{v}, t)$ is the single-particle distribution function at location $\mathbf{r}$, microscopic velocity $\mathbf{v}$ and time t, τ is the relaxation time and $g \equiv g(\mathbf{r}, \mathbf{v}, t)$ is the Boltzmann–Maxwell equilibrium distribution function:

$$g = \frac{\rho}{(2\pi RT)^{D/2}} \exp\left(-\frac{(\mathbf{v}-\mathbf{u})^2}{2RT}\right), \tag{2}$$

where R is the ideal gas constant and D is the dimension. The macroscopic variables (the density ρ, the velocity $\mathbf{u}$ and the temperature T) are the moments of the distribution function:

$$\rho = \int f d\mathbf{v}, \tag{3}$$

$$\rho\mathbf{u} = \int \mathbf{v} f d\mathbf{v}, \tag{4}$$

$$\frac{1}{2}\rho DRT = \frac{1}{2}\int (\mathbf{v}-\mathbf{u})^2 f d\mathbf{v}. \tag{5}$$

As proposed by He and Luo,[7,8] the set of discrete velocities selected in the present work is the result of a direct dicretisation of the continuous Boltzmann equation. This requires that a quadrature be used for the evaluation of the three preceeding integrals that appear in the equilibrium distribution function. Furthermore, the order of the quadrature must suit the accuracy required. For macroscopic applications, it is sufficient for the quadrature to satisfy exactly the macroscopic equations under the first-order Chapman–Enskog expansion. Under the low-Mach-number approximation, using a Gauss–Hermite quadrature,[9] this requires integrals of the form

$$I_n = \int \exp\left(-\frac{\mathbf{v}^2}{2RT}\right) P_n(\mathbf{v}) d\mathbf{v} \tag{6}$$

to be computed exactly, where P_n is any polynomial up to order 6 for isothermal applications and up to order 8 for thermal applications. Using a Cartesian decomposition, this procedure leads, for thermal applications, to a set of five discrete velocity co-ordinates and five quadrature weights for each dimension. These discrete velocities are $v_0 = 0$, $v_1 = -v_2 = \sqrt{(5-\sqrt{10})RT}$ and $v_3 = -v_4 = \sqrt{(5+\sqrt{10})RT}$ and the quadrature weights are

$$w_i = 2^6 5! \sqrt{2\pi RT} H_6\left(\frac{v_i}{\sqrt{2RT}}\right)^{-2}, \tag{7}$$

where H_6 is the sixth-order Hermite polynomial. In two dimensions for instance, the moments of the distribution function are evaluated as

$$\int \mathbf{v}^n f \, d\mathbf{v} = \int \exp\left(-\frac{\mathbf{v}^2}{2RT}\right) \frac{\mathbf{v}^n f}{\exp\left(-\frac{\mathbf{v}^2}{2RT}\right)} d\mathbf{v} \approx \sum_i \sum_j w_i w_j \frac{\mathbf{v_{i,j}}^n f_{i,j}}{\exp\left(-\frac{\mathbf{v_{i,j}}^2}{2RT}\right)}, \tag{8}$$

where $\mathbf{e_x}$ and $\mathbf{e_y}$ are the two unit vectors of the Cartesian co-ordinate system, $\mathbf{v_{i,j}} = v_i \mathbf{e_x} + v_j \mathbf{e_y}$ and $f_{i,j} \equiv f\left(\mathbf{r}, \mathbf{v_{i,j}}, t\right)$. As the quadrature order is high enough to ensure satisfaction of the macroscopic equations under the first-order Chapman–Enskog expansion, such a discrete-velocity model should lead to exact simulations of macroscopic gas dynamics, including energy conservation (but with a fixed Prandtl number because of the BGK approximation). However, this model cannot be implemented as is: the discrete velocities are functions of the local temperature and so are variable in space. The corresponding discretized version of the Boltzmann equation could therefore only be solved using cumbersome interpolation schemes in the velocity space. A first approximate solution could be to make a Taylor expansion of the equilibrium distribution function around a reference temperature T_{ref}. This raises to order ten the polynomials P_n for which I_n must be computed exactly. This requires seven discrete velocities for each dimension, thus severely increasing computation requirements. Another approximate solution was preferred, in which the discrete velocities are fixed, corresponding to a given reference temperature, but the quadrature weights are recomputed for an exponential ponderation function depending on the local temperature T. This local adjustment of the quadrature weights takes into account the fact that for macroscopic applications the distribution function is close to the equilibrium distribution at the local temperature. For this approximate thermal model, the discrete velocities are therefore $v_0 = 0$, $v_1 = -v_2 = \sqrt{(5-\sqrt{10})RT_{\text{ref}}}$ and $v_3 = -v_4 = \sqrt{(5+\sqrt{10})RT_{\text{ref}}}$ and the quadrature weights are obtained locally as the solutions of the following linear system:[9]

$$K_0 = \int e^{-\frac{v^2}{2RT}} \, dv = \sum w_i, \tag{9}$$

$$K_2 = \int v^2 e^{-\frac{v^2}{2RT}} \, dv = \sum w_i \, v_i^2, \tag{10}$$

$$K_4 = \int v^4 e^{-\frac{v^2}{2RT}} \, dv = \sum w_i \, v_i^4 \tag{11}$$

with $K_0 = \sqrt{2\pi RT}$, $K_2 = RTK_0$ and $K_4 = 3(RT)^2 K_0$. The solution of this system leads to following simple expressions for the local weights:

$$w_0 = K_0 - \frac{\left(v_1^2 + v_3^2\right) K_2 - K_4}{v_1^2 v_3^2}, \tag{12}$$

$$w_1 = \frac{v_3^2 K_2 - K_4}{2v_1^2\left(v_3^2 - v_1^2\right)}, \tag{13}$$

$$w_3 = \frac{K_4 - v_1^2 K_2}{2v_3^2\left(v_3^2 - v_1^2\right)}. \tag{14}$$

3. FINITE-DIFFERENCE IMPLEMENTATION AND TESTING

Numerical simulations were performed to test the validity of the above described discrete-velocity model. A classical Euler scheme is used for temporal integration and a second upwind finite-difference scheme is used for transport.[10] Boundary conditions are those of ref. 11. A series of academic simulation examples is presented below to illustrate the ability of the model to deal with compressibility and thermal effects. The first example concerns viscosity effects. We consider the decay of a vortex as described in ref. 12. The initial velocity conditions are:

$$u_x = (y_0 - y)\omega_0 \exp\left(-\frac{(\mathbf{r} - \mathbf{r}_0)^2}{L^2}\right), \tag{15}$$

$$u_y = (x - x_0)\omega_0 \exp\left(-\frac{(\mathbf{r} - \mathbf{r}_0)^2}{L^2}\right), \tag{16}$$

where $r_0 = (x_0, y_0)$ is the center of the vortex, L is the characteristic length of the initial vortex and ω_0 is the vorticity at the center. Figure 1 displays the analytical and simulated vorticity decays at vortex center, $\omega_{\max}$. The next two examples concern compressibility. Figure 2 shows the vertical density profile corresponding to stratification by gravity of an isothermal horizontal gas layer. Figure 3 shows the speed of sound evaluated by simulating propagation of a density wave. The last two examples concern thermal effects. Figure 4 illustrates simulation results for Couette flow and Fig. 5 shows estimated energy fluxes in a pure-conduction configuration. In all cases, the accuracy levels obtained in terms of density, velocity and temperature fields at the stationary limit are quite satisfactory. The points requiring more specific attention are the energy-flux estimations and the

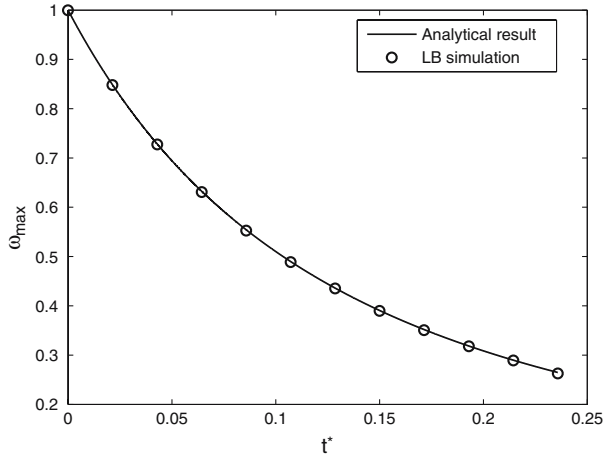

Fig. 1. Vorticity as a function of the dimensionless time $t^* = \nu t/L^2$ with $\nu = RT\tau$ the kinematic viscosity. The solid line represent the analytical result: $\omega_{\max}(t^*) = \omega_0/(1+4t^*)^2$. The crosses represent the LB simulations.

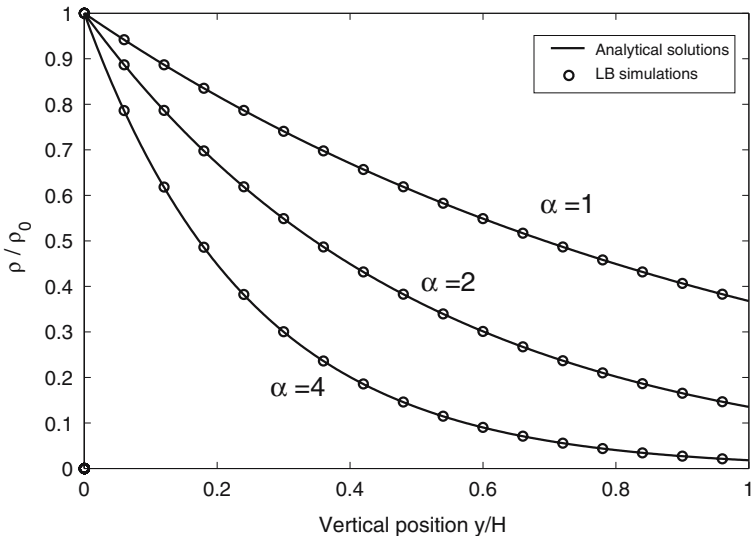

Fig. 2. A gravity force is introduced in the model as proposed by He *et al.*[13] Vertical density profiles are compared with analytical macroscopic solutions at the stationary limit for an isothermal gas layer of thickness H. Simulations are performed for three values of $\alpha = gH/RT$ where g is the acceleration due to gravity.

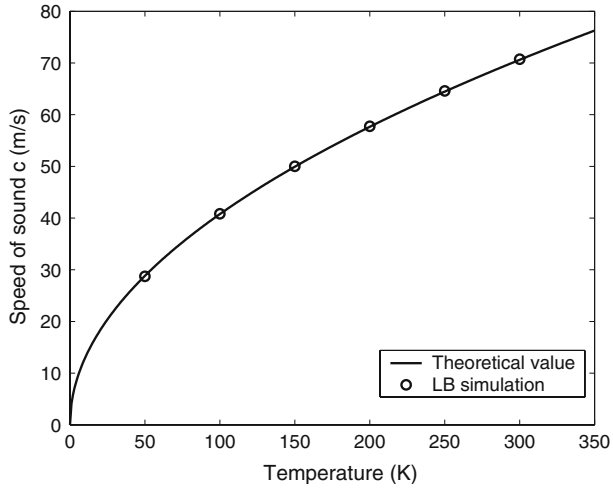

Fig. 3. The speed of sound was estimated for various temperatures and compared with the theoretical value $c = \sqrt{2RT}$. Following the idea proposed by Watari and Tsutahara,[10] the density distribution was initialized as a step profile with a small difference in density and the speed of sound is directly estimated by simple front tracking.

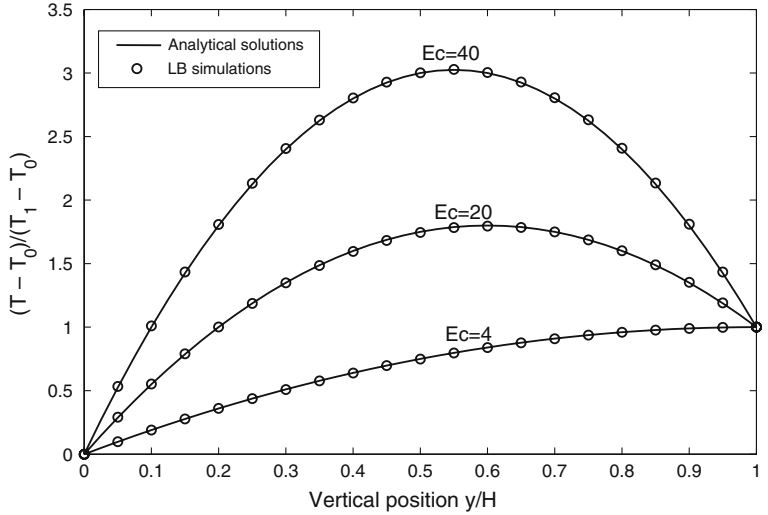

Fig. 4. Heat dissipation is tested in traditional Couette flow with a temperature gradient[5] for a gas layer of thickness H. The wall at location $y = 0$ is fixed and its temperature is T_0. The wall located at $y = H$ moves with a constant speed and its temperature is T_1. The simulation points are in complete agreement with the analytical solution for different Eckert numbers ($Ec = [4; 20; 40]$).

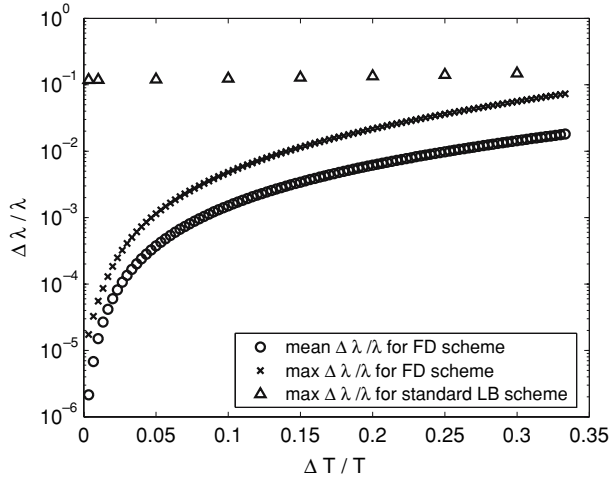

Fig. 5. The relative error in thermal conductivity is shown for different values of $\Delta T/T$. From the Chapman–Enskog expansion, the thermal conductivity is $\lambda = ((D+2)/2)R^2T\tau$. The mean (circles) and maximum (crosses) relative errors incurred using the finite-difference scheme tend asymptotically towards 0 for quasi-isothermal situations. The sensitivity to the reference temperature is indicated by the maximum error, as it occurs where the temperature is minimum or maximum, i.e., $T - T_{\text{ref}} = \Delta T/2$. However the maximum relative error inherent in a traditional lattice scheme (triangles) shows the presence of a residual error.

prediction of unstationary dynamics. The fact that discrete velocities are fixed at a reference temperature T_{ref} implies that, even though the quadrature weights are adjusted to the local temperature T, the quadrature order is not high enough for rigorous macroscopic simulations. The associated biases are therefore direct functions of the temperature difference $T - T_{\text{ref}}$. The simulation results reported in Fig. 5 indicate however that acceptable accuracy is obtained even for strong deviations from the reference temperature. Configurations with 10% temperature differences could be simulated with a 0.5% accuracy on energy fluxes at the stationary limit. Configurations with 30% temperature differences gave 5% accuracy in flux. The corresponding accuracy levels in terms of characteristic times in the unstationary phases are very similar.

Note. In the applications tested and even for very large temperature differences, the present model showed no pathological numerical instabilities. However, strong instabilities appeared (in accordance with the multi-speed thermal lattice Boltzmann literature[3]), when the quadrature weights were kept constant and spatially uniform at the values corresponding to the reference temperature. So adjusting the quadrature

weights to suit the local temperature seems useful in terms of numerical stability independently of accuracy considerations.

4. IMPLEMENTATION WITHIN THE STANDARD LATTICE BOLTZMANN ALGORITHM

When attempting to implement the above discrete-velocity model in standard lattice Boltzmann schemes, the first difficulty is that $v_3 \neq 2\,v_1$ and $v_4 \neq 2\,v_2$. Independent of the temperature, we find $v_3/v_1 = v_4/v_2 \approx 2.1$. Therefore, if the time step δt is adjusted so that information is exactly transported from one node to an adjacent node at speed v_1 (or v_2) during δt, then the information transported at speed v_3 (or v_4) does not fall exactly on the lattice. In order to bypass this difficulty with an approximate approach, we suggest imposing arbitrarily $v_3 = 2v_1$ and $v_4 = 2v_2$, and making use of the same quadrature weight adjustment as in Section 2, function of the local temperature. This leads to the following discrete velocity set: $v_0 = 0$, $v_1 = -v_2 = \sqrt{(5-\sqrt{10})RT_{\text{ref}}}$ and $v_3 = -v_4 = 2v_1$. The quadrature weights are those of Eq. (12). As already mentioned, such a procedure of weight adjustment for a fixed set of velocities does not ensure a high enough order of quadrature. Furthermore, unlike the velocity set derived with the Gauss–Hermite procedure, this scheme will not be precise in the limit of small temperature differences. In order to test the level of accuracy that can be achieved with such an approximate approach, this new discrete-velocity model is implemented in the following lattice Boltzmann scheme:[5]

$$\overline{f}\left(\mathbf{r}+\mathbf{v}_{i,j}\delta t, \mathbf{v}_{i,j}, t+\delta t\right) = \overline{f}\left(\mathbf{r}, \mathbf{v}_{i,j}, t\right) - \frac{\delta t}{\tau + 0.5\,\delta t}\left[\overline{f}\left(\mathbf{r}, \mathbf{v}_{i,j}, t\right) - g\left(\mathbf{r}, \mathbf{v}_{i,j}, t\right)\right] \tag{17}$$

with $\overline{f} = f + \frac{\delta t}{2\tau}(f-g)$. When the resulting lattice Boltzmann model is tested on the same five test cases as in Section 3, the accuracy achieved in terms of density, velocity and temperature fields in the stationary limit are quite similar to those obtained with the more accurate quadrature set and the finite-difference scheme. However the estimated energy fluxes and the characteristic times in the unstationary phases are much less accurate. In Fig. 5, the error on the energy flux does not vanish in the quasi-isothermal limit: a residual error of more than 10% is observed and similar biases are observed concerning temporal evolution.

5. CONCLUSIONS

For implementation in traditional lattice Boltzmann schemes, a degraded "double-speed" version of the proposed discrete velocity model can be used for approximate simulations. However, results are unsatisfactory in simulating energy flux. So far we have performed two complementary test studies to try to bypass this flux-estimation difficulty. In both cases, the idea was to go back to the accurate discrete velocity model of Section 2 using an interpolation procedure. In the first study, we interpolated $f_{i,j}$ outside the nodes in geometrical space. When a linear interpolation was used, strong numerical instabilities were observed. Practical simulations could only be performed with a quadratic interpolation.[6,14] The corresponding accuracy for energy-flux estimation is grid dependent and tends to that of the finite-difference scheme in the limit of an infinite number of nodes. We observed that residual errors lower than those of Section 4 could easily be reached with reasonable spatial meshing. In the second test study, the interpolation was performed in the velocity space so as to estimate the distribution function for the non-double speed assuming that f follows the Maxwellian form of the local equilibrium distribution function (cf. Appendix B). Here the accuracy is not lattice dependent: there was a 3% residual error for energy flux which is significantly better than the residual error of the above "double-speed" model. These last preliminary test studies were only performed in one dimension. For extension to two dimensions, difficulties arise in terms of boundary conditions.

On the whole, it can be concluded that using a finite-difference lattice Boltzmann scheme, excellent accuracy levels can be obtained with the set of five discrete velocities corresponding to the Gauss–Hermite quadrature, together with a local adjustment of the quadrature weights as a function of temperature. This could be performed without great difficulty because the finite-difference approach is not restricted to velocity sets that exactly link lattice nodes in one time step.

APPENDIX A. DETERMINATION OF QUADRATURE ORDER

For heat transfer applications, thermal fluxes must be correctly evaluated and therefore the moments of the distribution function must be correctly evaluated up to the third moment. Here the first-order Chapman–Enskog expansion is used to show that this constraint is equivalent to a correct evaluation of the first six moments of the local equilibrium distribution function (Section A.1). Under the low-Mach and low-ΔT

approximations, the equilibrium distribution function is written as the product of a centered Gaussian with a fourth order $\mathbf{v}$ polynomial (Section A.2), which leads to the use of 10th order Gauss–Hermite quadrature (Section A.3).

A.1. Chapman–Enskog Procedure

The Chapman–Enskog procedure is used to recover the macroscopic equations. This consists in expanding the distribution function f around the equilibrium function g and in evaluating the mean value of the product of the Boltzmann equation by all collisional invariants.

$$\int \chi \left(\frac{\partial f}{\partial t} + \mathbf{v} \cdot \nabla f \right) d\mathbf{v} = 0 \tag{A.1}$$

with χ a collisional invariant (1,$\mathbf{v}$ and $(1/2)\mathbf{v}^2$). At zero order, the integral (A.1) is evaluated with $f = g$ leading to the hydrodynamic equations for perfect fluids (without dissipative effects). To recover the dissipative terms, the distribution function f is expanded around the equilibrium function g.

$$f \approx g + f^{(1)}. \tag{A.2}$$

Replacing f in the Boltzmann equation by $g + f^{(1)}$ leads to:

$$\frac{\partial \left(g + f^{(1)} \right)}{\partial t} + \mathbf{v} \cdot \nabla \left(g + f^{(1)} \right) = -\frac{f^{(1)}}{\tau} \tag{A.3}$$

and neglecting $f^{(1)}$ on the left-hand side, $f^{(1)}$ may be written:

$$f^{(1)} \approx -\tau \left(\frac{\partial g}{\partial t} + \mathbf{v} \cdot \nabla g \right). \tag{A.4}$$

The temporal and spatial derivatives of g are direct functions of the spatial derivatives of ρ, u and T, which leads to:

$$\begin{aligned} f^{(1)} \approx -\tau g \Bigg\{ & \frac{1}{T} \left[(\mathbf{v} - \mathbf{u}) \cdot \nabla T \right] \left[\frac{(\mathbf{v} - \mathbf{u})^2}{2RT} - \frac{5}{2} \right] \\ & + \frac{1}{2RT} \left(\frac{\partial u_j}{\partial x_i} + \frac{\partial u_i}{\partial x_j} \right) \left[(v_i - u_i)(v_j - u_j) - \frac{1}{3} \delta_{ij} (\mathbf{v} - \mathbf{u})^2 \right] \Bigg\}. \end{aligned} \tag{A.5}$$

So, in the general case, $f^{(1)}$ can be written as $f^{(1)} \approx g \cdot P_3(\mathbf{v})$, and for isothermal applications $f^{(1)} \approx g \cdot P_2(\mathbf{v})$.

A.2. Equilibrium Expansion

For thermal applications, the equilibrium distribution function g is expanded around $u = 0$ (low-Mach-number approximation) and around $T = T_0$, where T_0 is a reference temperature.

$$
\begin{aligned}
g &= \frac{\rho}{(2\pi RT)^{D/2}} \exp\left(-\frac{(\mathbf{v}-\mathbf{u})^2}{2RT}\right) \\
&\approx \frac{\rho}{(2\pi RT)^{D/2}} \exp\left(-\frac{\mathbf{v}^2}{2RT}\right) \cdot \left[1 + \frac{\mathbf{v}\cdot\mathbf{u}}{RT} + \frac{(\mathbf{v}\cdot\mathbf{u})^2}{2(RT)^2} - \frac{\mathbf{u}^2}{2RT}\right] \\
&\approx \frac{\rho}{(2\pi RT)^{D/2}} \exp\left(-\frac{\mathbf{v}^2}{2R(T_0+\theta)}\right) \cdot \left[1 + \frac{\mathbf{v}\cdot\mathbf{u}}{RT} + \frac{(\mathbf{v}\cdot\mathbf{u})^2}{2(RT)^2} - \frac{\mathbf{u}^2}{2RT}\right] \\
&\approx \frac{\rho}{(2\pi RT)^{D/2}} \exp\left(-\frac{\mathbf{v}^2}{2RT_0}\right) \exp\left(\frac{\mathbf{v}^2}{2RT_0}\frac{\theta}{T_0}\right) \cdot \left[1 + \frac{\mathbf{v}\cdot\mathbf{u}}{RT} + \frac{(\mathbf{v}\cdot\mathbf{u})^2}{2(RT)^2} - \frac{\mathbf{u}^2}{2RT}\right] \\
&\approx \frac{\rho}{(2\pi RT)^{D/2}} \exp\left(-\frac{\mathbf{v}^2}{2RT_0}\right) \cdot \left(1 + \frac{\mathbf{v}^2}{2RT_0}\frac{\theta}{T_0}\right) \cdot \left[1 + \frac{\mathbf{v}\cdot\mathbf{u}}{RT} + \frac{(\mathbf{v}\cdot\mathbf{u})^2}{2(RT)^2} - \frac{\mathbf{u}^2}{2RT}\right] \\
&\approx \exp\left(-\frac{\mathbf{v}^2}{2RT_0}\right) \cdot P_4(\mathbf{v}) \qquad \text{(A.6)}
\end{aligned}
$$

with $\theta = T - T_0$, and $P_4(\mathbf{v})$ is a fourth-order $\mathbf{v}$ polynomial. So the equilibrium distribution function g is approximated by the product of centered Gaussian function with a fourth-order $\mathbf{v}$ polynomial.

A.3. Required Quadrature Orders

For thermal applications, moments of f are addressed up to the third: $\int P_3(\mathbf{v}) f \, d\mathbf{v}$. Then $f \approx g + f^{(1)} = g \cdot P_3(\mathbf{v})$ and $g \approx \exp(-\frac{\mathbf{v}^2}{2RT_0}) \cdot P_4(\mathbf{v})$. So the quadrature must evaluate the moments of a Gaussian function up to order 10: $\int P_{10}(\mathbf{v}) \exp(-\frac{\mathbf{v}^2}{2RT_0}) d\mathbf{v}$. For isothermal applications, only the first two moments of f are addressed. Then $f \approx g + f^{(1)} = g \cdot P_2(\mathbf{v})$ and $g \approx \exp(-\frac{\mathbf{v}^2}{2RT_0}) \cdot P_2(\mathbf{v})$. So the quadrature must evaluate the moments of a Gaussian function up to order 6: $\int P_5(\mathbf{v}) \exp(-\frac{\mathbf{v}^2}{2RT_0}) d\mathbf{v}$.

APPENDIX B. EXTRAPOLATION IN VELOCITY SPACE

The discrete velocity set corresponding to the Gauss–Hermite quadrature is such that $v_3 \neq 2v_1$ and $v_4 \neq 2v_2$ (cf. Fig. B.1). So, in one

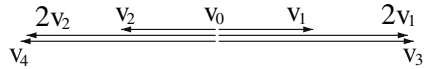

Fig. B.1. Discrete velocities set.

dimension, for the traditional lattice Boltzmann algorithm, we compute f_0, f_1, f_2, f_{2v_1} and f_{2v_2}. Then f_3 and f_4 are extrapolated assuming f_i has a Maxwellian form:

$$f_i \approx A \exp\left(-\frac{(v_i - B)^2}{C}\right). \tag{B.1}$$

To extrapolate f_3, the coefficients A, B and C are determined with f_0, f_1 and f_{2v_1} and to extrapolate f_4 another set of coefficients is used corresponding to f_0, f_2 and f_{2v_2}. Finally, the macroscopic variables ρ, u and T are calculated with f_0, f_1, f_2, f_3 and f_4.

REFERENCES

1. S. Chen and G. D. Doolen, *Ann. Rev. Fluid Mech.* **30**:329 (1998).
2. P. L. Bhatnagar, E. P. Gross, and M. Krook, *Phys. Rev.* **94**:511 (1954).
3. G. McNamara, A. L. Garcia, and B. J. Alder, *J. Stat. Phys.* **81**:395 (1995).
4. X. Shan, *Phys. Rev. E* **55**:2780 (1997).
5. X. He, S. Chen, and G. D. Doolen, *J. Comput. Phys.* **146**:282–300 (1998).
6. G. Vahala, P. Pavlo, L. Vahala, and N. Martys, *J. Modern Phys. C* **9**:1247–1261 (1998).
7. X. He and L.-S. Luo, *Phys. Rev. E* **55**:R6333 (1997).
8. X. He and L.-S. Luo, *Phys. Rev. E* **56**:6811 (1997).
9. P. J. Davis and P. Rabinowitz, *Methods of Numerical Integration*, 2nd ed. (Academic, New York, 1984).
10. M. Watari and M. Tsutahara, *Phys. Rev. E* **67**:036306 (2003).
11. M. Watari and M. Tsutahara, *Trans. Jpn. Soc. Mech. Eng. B* **68**:676 (2002).
12. M. Bouzidi, D. d'Humières, P. Lallemand, and L.-S. Luo, *J. Comput. Phys.* **172**:704 (2001).
13. X. He, X. Shan, and G. D. Doolen, *Phys. Rev. E* **57**:R13 (1998).
14. P. Pavlo, G. Vahala, and L. Vahala, *Phys. Rev. Lett.* **80**:3960 (1998).